Research Article | Vol. 30, No. 7 / 28 Mar 2022 / Optics Express 11317
Optics EXPRESS

Entangled photons from composite cascade emitters

DEREK S. WANG,[1,4,*] İNCİ ANALI,[2,4] AND SUSANNE F. YELIN[3]

[1]Harvard John A. Paulson School of Engineering and Applied Sciences, Harvard University, Cambridge, MA 02138, USA
[2]Harvey Mudd College, Claremont, CA 91711, USA
[3]Department of Physics, Harvard University, Cambridge, MA 02138, USA
[4]These authors contributed equally to this work.
[*]derekwang@g.harvard.edu

Abstract: One of the most versatile sources for entangled photons are emitters that interact via more than one tunable mechanism. Here, we demonstrate how hybridization and dipole-dipole interactions—potentially simultaneously available in colloidal quantum dots and molecular aggregates—leveraged in conjunction can couple simple, well understood emitters into composite emitters with flexible control over the level structure. We show that cascade decay through carefully designed level structures can result in emission of frequency-entangled photons with Bell states and three-photon GHZ states as example cases. These results pave the way toward rational design of quantum optical emitters of entangled photons.

1. Introduction

Entanglement, especially among photonic qubits, is not only useful for testing the limits of quantum theory [1–5], but also a valuable resource in photonic quantum technologies, such as quantum computers and quantum networks [5–9]. For instance, Bell states, or maximally entangled photon pairs, are necessary for quantum teleportation, the fundamental mechanism by which quantum repeaters send quantum information over long distances [7]; three-qubit maximally entangled GHZ states are useful for quantum cryptography and secret sharing [8]; and cluster states, or highly entangled states of many qubits, underlie measurement-based quantum computing that is formally equivalent to more traditional quantum circuit-based models but requires only easy-to-implement single-qubit gates upon successful creation of a cluster state [9].

Despite the ubiquitous need for entangled photons in quantum technologies, producing them with high fidelity, quickly, and deterministically—even just pairs of photons—remains a challenge. Relatively successful approaches for producing pairs of entangled photons include spontaneous parametric down-conversion [10–14] or four-wave mixing [15,16], but the number of photon pairs generated follows a Poissonian distribution [17], rendering both the pair generation efficiency and rate too slow for scalable quantum systems [5]. Another approach uses semiconductor quantum dots to deterministically emit entangled photon pairs *via* biexciton decay cascade [18–26]. Generalizing this approach to produce higher-order, multi-photon entangled states with fine control over the entanglement basis remains difficult, however, driving long-standing and active research into alternative approaches [27–32] that so far require complex, active control over photon emitters.

In addition, many of these previous proposals only consider entanglement in the photon polarization basis. Encoding in the frequency basis, however, offers several advantages for certain quantum technological applications, such as in quantum networking, where, for instance, optical photon frequencies are more suitable for on-chip computation while mid-infrared frequencies transmit more efficiently through fibers for quantum communication [5,20,33–36].

#452935 https://doi.org/10.1364/OE.452935
Journal © 2022 Received 5 Jan 2022; revised 9 Mar 2022; accepted 9 Mar 2022; published 21 Mar 2022

Optics EXPRESS

The continuous frequency degree also offers the opportunity for encoding higher-dimensional quantum information, *e.g.* qudits instead of qubits [37].

In this study, we demonstrate how to design the level structures of composite quantum emitters for deterministic emission of entangled photons *via* cascade decay. Rather than coupling single emitters through just the longer-range dipole-dipole coupling interaction, we also consider the shorter-range hybridization interaction. At intermediate distances between emitters, both types of interaction can be simultaneously relevant, such as in moiré excitons [38], molecular aggregates [39], and quantum dots [40]. We show that the two types of interactions lead to qualitatively different types of state mixing and that this difference can be leveraged to generate a level structure amenable to emission of two-photon Bell states from just two two-level emitters. We also show that this approach can be generalized to higher-order entangled states by designing a system consisting of three emitters that is capable of emitting three-photon GHZ states with fidelity $\mathcal{F}$ as high as 90% and efficiency $\eta = 0.55$. We anticipate these results will motivate research into designing composite emitters for emission of entangled photons from real emitters with multiple interactions of different character, especially molecular aggregates and colloidal quantum dots.

2. Theoretical formalism

Here, we introduce the theoretical formalism for computing the level structure, or eigenenergies E_l and dipole-allowed transitions between eigenstates l and m indicated by non-zero transition dipole moment $|\boldsymbol{d}_{lm}|$, of NM-level emitters interacting *via* dipole-dipole and hybridization interactions. For simplicity, we set $M = 2$ throughout, *i.e.* we study ensembles of two-level emitters.

Each emitter i is comprised of a ground orbital $|g_i\rangle$ and an excited orbital $|e_i\rangle$ with energy $\hbar\omega_i$, transition dipole moment $\boldsymbol{d}_i = \langle g_i|\mathrm{e}\hat{\boldsymbol{r}}|e_i\rangle$, and position $\boldsymbol{r}_i$, where $\hbar$ is the reduced Planck constant, e is the electron charge and $\hat{\boldsymbol{r}}$ is the position operator. We assume each orbital can be occupied by one electron. Therefore, in the number basis $|N_i^g, N_i^e\rangle$, there are four possible states: $|0_i^g, 0_i^e\rangle$, $|0_i^g, 1_i^e\rangle$, $|1_i^g, 0_i^e\rangle$, and $|1_i^g, 1_i^e\rangle$.

The total Hamiltonian $\hat{H}$, including dipole-dipole and hybridization interactions, can be written as:

$$\hat{H} = \hat{H}_0 + \hat{H}_{\mathrm{dip}} + \hat{H}_{\mathrm{hyb}}. \tag{1}$$

The bare-emitter Hamiltonian is $\hat{H}_0 = \sum_i^N \hat{H}_i$, where the isolated emitter Hamiltonian $\hat{H}_i = \hbar\omega_i \hat{a}_{e,i}^\dagger \hat{a}_{e,i}$, and $\hat{a}_{o,i}^\dagger$ ($\hat{a}_{o,i}$) is the creation (annihilation) operator for an electron in orbital $o \in \{g, e\}$ of emitter i. The bare-emitter Hamiltonian $\hat{H}_0$ can be augmented to incorporate single-emitter binding as $\hat{H}_{\mathrm{bind}} = \sum_i^N K_i a_{e,i}^\dagger a_{g,i}^\dagger a_{e,i} a_{g,i}$; we explore this effect in Appendix A, where we show that binding energies must be smaller than dipole-dipole and hybridization energies for high-fidelity emission of Bell states.

The dipole-dipole interaction is a well explored method of coupling together single emitters to create composite emitters capable of, for instance, emission of entangled photon pairs [41], implementation of multi-photon quantum logic gates [42,43], and superradiance [44]. This Hamiltonian is

$$\hat{H}_{\mathrm{dip}} = \sum_{i,j>i}^{N} J_{ij} \hat{\boldsymbol{d}}_i \hat{\boldsymbol{d}}_j, \tag{2}$$

where $\hat{\boldsymbol{d}}_i = \boldsymbol{d}_i(\hat{a}_{e,i}^\dagger \hat{a}_{g,i} + \hat{a}_{g,i}^\dagger \hat{a}_{e,i})$ is the dipole operator. We retain all double (de-)excitations to preclude limitations of the rotating wave approximation. J_{ij} is the dipole interaction energy given by

$$J_{ij} = \frac{|\boldsymbol{d}_i||\boldsymbol{d}_j||}{4\pi\epsilon_0\epsilon_r|\boldsymbol{r}_i - \boldsymbol{r}_j|^3}\left[\boldsymbol{n}_i \cdot \boldsymbol{n}_j - 3(\boldsymbol{n}_i \cdot \boldsymbol{n}_{ij})(\boldsymbol{n}_j \cdot \boldsymbol{n}_{ij})\right], \tag{3}$$

where ϵ_r is the relative permittivity, $\boldsymbol{n}_i$ is the unit vector of the dipole moment $\boldsymbol{d}_i$, and $\boldsymbol{n}_{ij}$ is the unit vector of $\boldsymbol{r}_i - \boldsymbol{r}_j$. This form of the dipole-dipole interaction is appropriate only when the

Optics EXPRESS

dipole-dipole distance $|\mathbf{r}_i - \mathbf{r}_j|$ is smaller than the transition wavelength λ in a medium with relative permittivity ϵ_r [45]. States that are dark under this approximation can, in fact, emit radiation with the full form of the dipole-dipole interaction. We quantitatively estimate the impact of this approximation for the parameters studied here in Appendix B. In addition, J_{ij} can be re-scaled by Dexter exchange coupling [46] at short inter-emitter distances less than 20 atomic units (Bohr), the lowest value considered in this study.

The hybridization interaction Hamiltonian is

$$\hat{H}_{\text{hyb}} = \sum_{i,j>i}^{N} G^{\text{e}}_{ij}(\hat{a}^{\dagger}_{e,i}\hat{a}_{e,j} + \hat{a}^{\dagger}_{e,j}\hat{a}_{e,i}). \tag{4}$$

where G^{e}_{ij} is the hybridization interaction energy between excited orbitals $|e_i\rangle$ and $|e_j\rangle$. This interaction is akin to inter-emitter electron, or charge, transfer that has been well studied in the molecular aggregates [39] and exciton communities [47]. While G^{e}_{ij}, like J_{ij}, is dependent on the inter-emitter distance $|\boldsymbol{r}_i - \boldsymbol{r}_j|$, in this study we fix the inter-emitter distances and directly vary G^{e}_{ij}, physically corresponding to the strong dependence of the wavefunction overlap on the shape or principal number of the orbitals. Note that we ignore hybridization interactions between orbitals $|e_i\rangle$ and $|g_j\rangle$ because they are distant in energy, as well as interactions between ground orbitals $|g_i\rangle$ and $|g_j\rangle$ because the ground orbitals of real emitters of interest are often tightly localized. In principle, however, one can add, for instance, the ground orbital hybridization term $\sum_{i,j>i}^{N} G^{g}_{ij}(\hat{a}^{\dagger}_{g,i}\hat{a}_{g,j} + \hat{a}^{\dagger}_{g,j}\hat{a}_{g,i})$ to $\hat{H}_{\text{hyb}}$; the impact of this term is further studied in Appendix C.

Finally, we determine the level diagram of N two-level emitters by diagonalizing H and transforming the total dipole operator $\hat{\boldsymbol{d}} = \sum_i \hat{\boldsymbol{d}}_i$ into the eigenbasis. With the level diagram, we can evaluate the quality, specifically the efficiency η and fidelity $\mathcal{F}$, of the emitted photons *via* cascade decay from multiply excited states of cascade emitters, as described in Appendix D.

3. Entanglement

3.1. Asymmetric mixing for Bell states

We explain why the combination of both dipole-dipole and hybridization interactions enable fuller control over the level diagram of N two-level emitters, including those that are amenable to the emission of entangled photons. As an example, we study in detail the simple scenario illustrated in Fig. 1(a), where $\boldsymbol{r}_1 - \boldsymbol{r}_2 = r_x\hat{i}$ and $\hbar\omega = \hbar\omega_1 = \hbar\omega_2$. We also assume the angle θ between the x-axis and the transition dipole moment of the second emitter is 0, so that $\boldsymbol{d}_1 = \boldsymbol{d}_2 = d_x\hat{i}$. Finally, with two electrons in the system, there are 6 possible states in the number basis $|N^g_1, N^e_1, N^g_2, N^e_2\rangle$. For notational convenience, we label these number states as, *e.g.*, $|0^g_1, 0^e_1, 1^g_2, 1^e_2\rangle \equiv |g_2e_2\rangle$, where only the occupied orbitals are included.

First, to understand the role of dipole-dipole coupling, we plot the level diagram without hybridization ($\hat{H} = \hat{H}_0 + \hat{H}_{\text{dip}}$) on the left of Fig. 1(b). In this well known result, the eigenstates $|l\rangle$ and eigenenergies E_l, in order of increasing E_l, are as follows: ground state $|g\rangle \approx |g_1g_2\rangle$ with $E_g \approx 0$; symmetric bright state $|S\rangle \approx 1/\sqrt{2}(|e_1g_2\rangle + |g_1e_2\rangle)$ with $E_S \approx \hbar\omega - |J_{12}|$; two states $|g_2e_2\rangle$ and $|g_1e_1\rangle$ corresponding to double occupation of emitter 1 and 2, respectively, both with energy of $\hbar\omega$; anti-symmetric dark state $|A\rangle \approx 1/\sqrt{2}(|e_1g_2\rangle - |g_1e_2\rangle)$ with $E_A \approx \hbar\omega + |J_{12}|$; and doubly excited state $|ee\rangle \approx |e_1e_2\rangle$ with $E_{ee} \approx 2\hbar\omega$. Note that the energies E_l are generally listed here with their approximate values as opposed to exact ones due to the inclusion of the double excitation and de-excitation terms. The dipole coupling mixes only two of the singly excited states $|e_1g_2\rangle$ and $|g_1e_2\rangle$ with each other. Assuming that the doubly excited state $|ee\rangle$ is initially populated *via*, for instance, two-photon absorption [41], the only dipole-allowed cascade decay path is $|ee\rangle \rightarrow |S\rangle \rightarrow |g\rangle$, emitting two unentangled photons.

Now we seek understanding of the role of the hybridization interaction in the level diagram by plotting the level diagram without dipole-dipole coupling ($\hat{H} = \hat{H}_0 + \hat{H}_{\text{hyb}}$) on the right

Optics EXPRESS

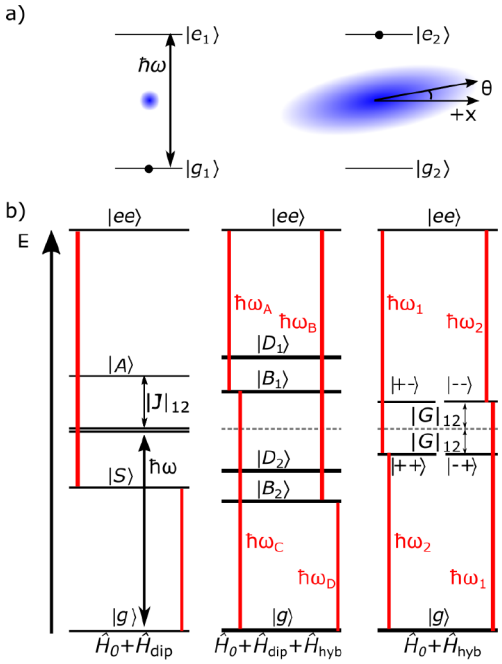

Fig. 1. a) Schematic of $N = 2$ two-level emitters on the x-axis with transition dipole moments $\boldsymbol{d}_1 = d_x\hat{i}$ and $\boldsymbol{d}_2 = d_x[\cos(\theta)\hat{i} + \sin(\theta)\hat{j}]$. We assume the wave functions of the ground state are tightly localized, while the excited state are delocalized enough to interact through the hybridization interaction. The smaller blue circle and larger blue ellipse are pictorial representations of the ground and excited state wave functions, respectively. b) Level diagrams for $N = 2$ two-level emitters for $\hat{H} = \hat{H}_0 + \hat{H}_{\text{dip}}$ (left), $\hat{H} = \hat{H}_0 + \hat{H}_{\text{dip}} + \hat{H}_{\text{hyb}}$ (middle), and $\hat{H} = \hat{H}_0 + \hat{H}_{\text{hyb}}$ (right). Allowed transitions, or those with non-zero transition dipole moments, *via* cascade decay from the doubly excited state $|ee\rangle$ are in red. Emission of frequency-entangled Bell states is only possible for two two-level emitters with both dipole-dipole and hybridization interactions.

of Fig. 1(b). The level diagram is as follows when $G_{12}>0$: ground state $|g\rangle = |g_1g_2\rangle$ with $E_g = 0$; $|++\rangle = 1/2(|g_1\rangle + |g_2\rangle)(|e_1\rangle + |e_2\rangle)$ and $|-+\rangle = 1/2(|g_1\rangle - |g_2\rangle)(|e_1\rangle + |e_2\rangle)$ with $E_{++} = E_{-+} = \hbar\omega - |G_{12}|$; two singly excited states $|+-\rangle = 1/2(|g_1\rangle + |g_2\rangle)(|e_1\rangle - |e_2\rangle)$ and $|--\rangle = 1/2(|g_1\rangle - |g_2\rangle)(|e_1\rangle - |e_2\rangle)$ with $E_{--} = E_{+-} = \hbar\omega + |G_{12}|$; and doubly excited state $|ee\rangle = |e_1e_2\rangle$ with $E_{ee} = 2\hbar\omega$. The hybridization interaction mixes all four of the singly excited states by allowing electrons to hop between emitters 1 and 2. In this case, there are two possible decay paths. At first blush this cascade decay may seem appropriate for emission of entangled photons. However, due to the equally weighted mixing between all four singly excited states, $\hbar\omega_1 = \hbar\omega_4$ and $\hbar\omega_2 = \hbar\omega_3$, the two photons emitted by the pathway on the left are the same as the photons emitted on the right, resulting in zero entanglement.

For emission of frequency-entangled photon pairs, another interaction, such as dipole-dipole coupling, is required to asymmetrically shift the bright eigenstates of $\hat{H} = \hat{H}_0 + \hat{H}_{\text{hyb}}$. We plot this scenario in the center of Fig. 1(b), where the eigenstates are $|g\rangle$, bright states $|B_1\rangle$ and $|B_2\rangle$, dark states $|D_1\rangle$ and $|D_2\rangle$, and $|ee\rangle$. The allowed transitions $|ee\rangle \rightarrow |B_1\rangle \rightarrow |g\rangle$ and $|ee\rangle \rightarrow |B_2\rangle \rightarrow |g\rangle$ all emit photons with unique frequencies from each other, enabling emission of a Bell state.

Optics EXPRESS

3.2. Entanglement optimization

We optimize the entanglement by tuning the system parameters in Fig. 2(a)-(c), respectively. Efficient evaluation of the level diagrams for cascade emission of entangled photons involves explicit time propagation of the excited electronic system with the Lindblad master equation, followed by generation of the off-diagonal elements of the photon density matrix through the quantum regression theorem and of the diagonal elements with a classical rate equation approach. This method is discussed in further detail in Appendix D. In particular, we determine the impact of these parameters on fidelity $\mathcal{F}$ with and efficiency η of emitting an ideal Bell state $|\phi_B\rangle = 1/\sqrt{2}(|0_1^L 0_2^L\rangle + |1_1^L 1_2^L\rangle)$, where the logical basis states $|0_1^L\rangle$ ($|0_2^L\rangle$) and $|1_1^L\rangle$ ($|1_2^L\rangle$) correspond to single-photon states with frequencies ω_A (ω_C) and ω_B (ω_D), respectively. We also plot the minimum energy difference ΔE_{min} between all emitted photons that are mapped onto the logical basis states. By doing so, we determine the maximum line broadening permissible to resolve photons from each other *via* their frequencies.

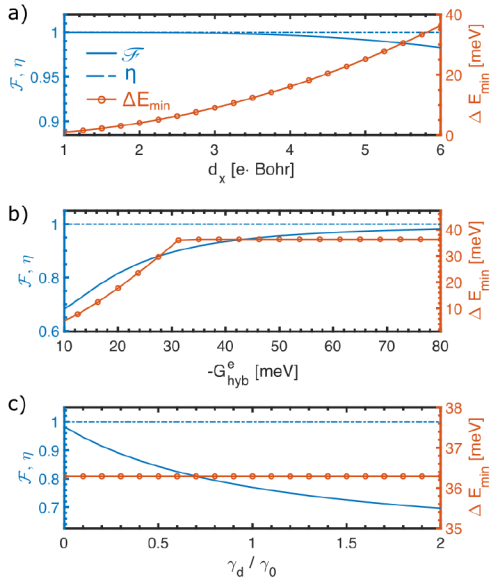

Fig. 2. We sweep (a) the magnitude of the transition dipole moment d_x, (b) the excited state hybridization interaction energy G^e_{hyb}, and (c) the dephasing rate γ_d relative to the fastest radiative decay rate $\max(\gamma_r^{lm})$. In each subplot, we show the fidelity $\mathcal{F}$ (solid blue) with an ideal Bell state, efficiency η (dotted blue), and ΔE_{min} (solid orange), or the minimum energy difference between emitted photons mapped onto logical basis states to determine the maximal photon peak broadening permissible for frequency resolution. All system parameters not being sweep in each respective plot are as follows: $\hbar\omega = 1$ eV, $d_x = |\boldsymbol{d}_1| = |\boldsymbol{d}_2| = 6$ e·Bohr, $\boldsymbol{r}_1 - \boldsymbol{r}_2 = 40\hat{i}$ in Bohr, $G^e_{hyb} = 80$ meV, and $\epsilon_r = 1$. Increasing the magnitude of the hybridization interaction increases $\mathcal{F}$ and ΔE_{min}. Meanwhile, increasing the dipole-dipole interaction *via* increasing d_x decreases $\mathcal{F}$ but eases the challenge of resolving the photon frequencies due to increasing ΔE_{min}. Decoherence rates on the order of and higher than the emission rate reduces entanglement fidelity.

We first sweep the magnitude of the transition dipole moment d_x in Fig. 2(a). Throughout this range, η remains 1, suggesting that all of the population follows the two decay paths resulting in the two superpositioned states in the Bell state. As d_x increases, ΔE_{min} increases to ~36 meV at $d_x = 6$ e·Bohr, while $\mathcal{F}$ decreases from 1 to 0.97; the former can be understood as a result of the

Optics EXPRESS

increasing dipole-dipole interaction energy, while the latter is a result of the two decay paths having increasingly different magnitudes of weights.

In Fig. 2(b), we then analyze the effect of changing the hybridization energy $G^{\mathrm{e}}_{\mathrm{hyb}}$. Throughout this range, η remains 1. With increasing hybridization magnitude, the fidelity $\mathcal{F}$ increases, while the ΔE_{min} increases until ~36 meV. $\mathcal{F}$ increases with increasing magnitude of G^{e}_{hyb} for a fixed dipole-dipole interaction because the weights of the two decay paths equalize, highlighting the importance of the additional presence of the hybridization interaction. ΔE_{min} saturates at ~36 meV with increasing magnitude of G^{e}_{hyb} because at that point, it is limited by the dipole-dipole interaction—recall that at $d_x = 6$ e·Bohr in Fig. 2(a), the same value of d_x in Fig. 2(b), $\Delta E_{\mathrm{min}} \sim 36$ meV.

Finally, in Fig. 2(c), we plot the effect of dephasing γ_{d} as a proportion of the bare emitter decay rate $\gamma_0 = Cd_x^2$ where $d_x = 6$ e·Bohr. Both η and ΔE_{min} remain constant, as expected because pure decoherence should not change the central emission frequency nor result in population loss. The fidelity $\mathcal{F}$, meanwhile, is sensitive to γ_{d}, validating the physical intuition that high-quality quantum emission requires fast radiative decay rates relative to environment loss and decoherence.

3.3. *Arbitrarily entangled photons: GHZ states*

The present method can be generalized to construct level structures for emission of arbitrary entangled photon states. As an example, we optimize the configuration in Fig. 3(a) for emission of a three-photon GHZ state $1/\sqrt{2}(|000\rangle + |111\rangle)$. All three two-level emitters lie on the x-axis with equal magnitude dipole moments that we assume to be in the x-direction for all three emitters, resulting in $>10^5$ possible decay paths.

We tune the system parameters in Fig. 3(a)-(d), respectively. In Fig. 3(b) and (c), we see that the maximum η is only around 0.9 with a significantly lower $\mathcal{F} = 0.55$. While the quality of entanglement is low, interestingly, all entanglement measures are much more stable with respect to changes in both d_x and $G^{\mathrm{e}}_{\mathrm{hyb}}$ compared to the Bell state structures studied in Fig. 2. For instance, in (c), $\mathcal{F}$ and η change by less than 1% and ΔE_{min} is stable within 0.1 meV. While we expect further improvements to be possible with multi-dimensional optimization techniques, these results already demonstrate the tantalizing promise of high-efficiency, high-fidelity, deterministic emission of arbitrary entangled photon states.

Finally, we briefly discuss typical values of system parameters explored in the present study. In molecular aggregates, dipole-dipole interactions interactions can be on the order of 1 meV [48,49]. In colloidal quantum dots, a recent experimental study showed a red-shift of approximately 15 meV [44] attributed to dipole-dipole coupling, and colloidal quantum dot molecules have exhibited hybridization interactions in the tens of meV [40]. Colloidal quantum dots in the nanoplatelet morphology can exhibit radiation-limited linewidths [50], where $\gamma_d/\gamma_0 \ll 1$. More typically, however, colloidal quantum dots have radiative rates on the order of 1 ns with dephasing rates of 100 ps [51]. As we show in the Appendix, however, binding energies must be much smaller than dipole-dipole and hybridization energies for realization of our theoretical proposal. In colloidal quantum dots, computational studies predict binding energies as low as tens of meV [52], suggesting low entanglement quality without further careful engineering of the quantum dots.

Optics EXPRESS

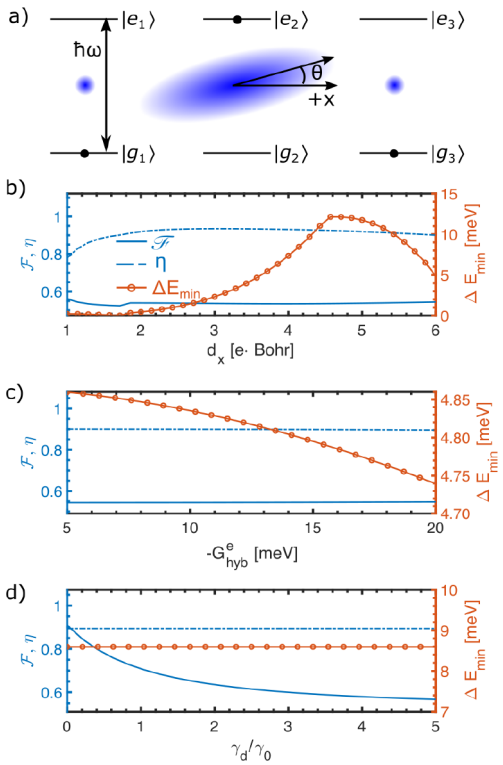

Fig. 3. (a) Configuration for $N = 3$ two-level emitters positioned on a line parallel to their dipole moments $\boldsymbol{d}_i$ and capable of emitting frequency-entangled GHZ states *via* cascade decay from the triply excited state $|20\rangle$. We sweep (b) d_x, (c) $G^{\mathrm{e}}_{\mathrm{hyb}}$, and (d) γ_{d}. All system parameters not being sweep in each respective plot are assumed to be as follows: $\hbar\omega = 1$ eV, $d_x = |\boldsymbol{d}_1| = |\boldsymbol{d}_2| = |d_3| = 6$ e·Bohr, $\boldsymbol{r}_3 - \boldsymbol{r}_2 = \boldsymbol{r}_1 - \boldsymbol{r}_2 = 20\hat{i}$ in Bohr , $G^{\mathrm{e}}_{\mathrm{hyb}} = 80$ meV, and $\epsilon_r = 1$. By optimizing the system parameters, $\mathcal{F}$ and η can be as high as 90% and 55% with $\Delta E_{\mathrm{min}} \sim 10$ meV.

4. Conclusions and outlook

In summary, we leverage hybridization and dipole-dipole interactions between simple emitters to construct composite emitters. These composite emitters have particularly valuable applications as deterministic sources of frequency-entangled photon states *via* cascade decay from multiply excited states. As two simple examples, we study two and three two-level emitters for emission of Bell and GHZ states, respectively. We explain why varying system parameters, including the strength of the hybridization interaction $G^{\mathrm{e}}_{\mathrm{hyb}}$ and direction and magnitude of the transition dipole moment $\boldsymbol{d}_{lm}$, affects three relevant metrics of the emitted entangled photons: fidelity $\mathcal{F}$, efficiency η, and minimum energy difference ΔE_{min} between emitted photons. For the GHZ state, we achieve a fidelity $\mathcal{F}$ and efficiency η as high as 90% and 55% with ΔE_{min} on the order of meV using reasonable parameters. Importantly, system-specific dephasing rates leading to inhomogenous broadening, such as vibrational and charge noise, must be much slower than the emission rate for high-fidelity emission. Future studies should consider system-dependent challenges, such as efficient pumping of highly excited states, as has been explored extensively in epitaxial quantum dots [53–58], and interaction-dependent loss and decoherence channels, as has been extensively studied for atoms [59].

Optics EXPRESS

Associated content

Code to reproduce the calculations in this paper are available at [60].

Appendix A. Binding interaction

Especially in molecular aggregates, the binding interaction term $\hat{H}_{\text{bind}} = \sum_i^N K_i a_{e,i}^\dagger a_{g,i}^\dagger a_{e,i} a_{g,i}$ that accounts for interactions between electrons of a fully occupied two-level system can be much larger than the dipole-dipole and hybridization interaction energies [39]. Explicitly, in the case of two identical two-level systems for emission of Bell states, we find that the energies of the bare states $|g_1 e_1\rangle$ and $|g_2 e_2\rangle$ that otherwise interact only *via* the hybridization interaction are greater than the energies of the states $|g_1 e_2\rangle$ and $|e_1 g_2\rangle$ that interact *via* both the hybridization and dipole-dipole interactions. Because these states are no longer degenerate, the hybridization interaction is less effective at asymmetrically mixing the singly excited states, resulting in poor overall entanglement emission, as we demonstrate in Fig. 4.

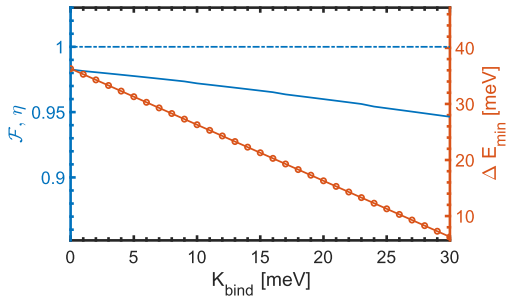

Fig. 4. Binding energy vs. fidelity $\mathcal{F}$ (solid blue) with an ideal Bell state, efficiency η (dotted blue), and ΔE_{min} (solid orange). $\hbar\omega = 1$ eV, $d_x = |\boldsymbol{d}_1| = |\boldsymbol{d}_2| = 6$ e·Bohr, $\boldsymbol{r}_1 - \boldsymbol{r}_2 = 40\hat{i}$ in Bohr, $G^e_{\text{hyb}} = 80$ meV, and $\epsilon_r = 1$. Increasing binding energy results in less effective asymmetric mixing of the hybridization interaction, lowering the entanglement quality.

Appendix B. Dipole-dipole interaction

The form of the dipole-dipole interaction in Eq. (3) is valid only when the inter-emitter distance $|\mathbf{r}_i - \mathbf{r}_j| = r_{ij}$ is much smaller than the bare-atom transition wavelength λ_0, or $r_{ij}/\lambda_0 = \xi \ll 1$ [45]. For concreteness, we quantitatively estimate the impact of this approximation on the results for the case of two two-level emitters, as in Fig. 1 and 2, noting that similar arguments can be made for more complex systems, such as the case of three two-level emitters in Fig. 3. We adapt the notation of Ref. [61].

Under the full expression for the dipole-dipole interaction, the anti-symmetric dark state can, in fact, emit photons with rate $\gamma_{\text{A}} = \Gamma[1 - F(\xi)]$, while the symmetric bright state with emission rate $\gamma_{\text{S}} = \Gamma[1 + F(\xi)]$ is less bright than under the approximated form, where $\Gamma = C|\mathbf{d}_1|^2 = C|\mathbf{d}_2|^2$ is the bare-emitter radiative decay rate, and $F(\xi)$ is the correction factor defined as

$$F(\xi) = \frac{3}{2}\Big[(1 - \cos^2\theta)\frac{\sin\xi}{\xi} \tag{5a}$$

$$+(1 - 3\cos^2\theta)\Big(\frac{\cos\xi}{\xi^2} - \frac{\sin\xi}{\xi^3}\Big)\Big]. \tag{5b}$$

In the case of two two-level emitters, $r_{ij} \sim 2$ nm with bare-emitter transition wavelengths $\lambda_0 \sim 1200$ nm, giving $F(\xi) \sim 0.99999$ and implying that the entanglement measures $\mathcal{F}$ and η are substantially more sensitive to the studied system parameters $d_x, G^{\text{e}}_{\text{hyb}}, \theta$, and γ_{d} than the neglected emission from dark states.

Optics EXPRESS

Appendix C. Ground-state hybridization

In Fig. 5, we include the ground-state hybridization term $\sum_{i,j>i}^{N} G_{ij}^{g}(\hat{a}_{g,i}^{\dagger}\hat{a}_{g,j} + \hat{a}_{g,j}^{\dagger}\hat{a}_{g,i})$ to $\hat{H}_{\text{hyb}}$ in addition to the excited-state hybridization term included in the remainder of the text and note qualitatively similar results, except that the fidelity reaches its plateau at a smaller $-G_{\text{hyb}}^{\text{e}} = -G_{\text{hyb}}^{\text{g}}$.

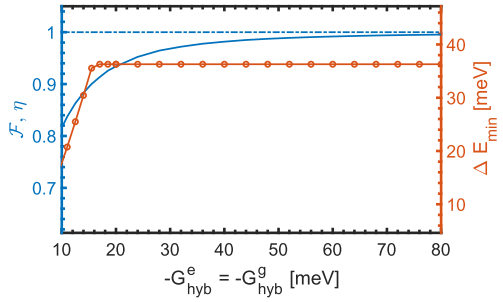

Fig. 5. Ground-state hybridization vs. fidelity $\mathcal{F}$ (solid blue) with an ideal Bell state, efficiency η (dotted blue), and ΔE_{min} (solid orange). $\hbar\omega = 1$ eV, $d_x = |\boldsymbol{d}_1| = |\boldsymbol{d}_2| = 6$ e·Bohr, $\boldsymbol{r}_1 - \boldsymbol{r}_2 = 40\hat{\imath}$ in Bohr, and $\epsilon_r = 1$. Non-zero ground state hybridization enables asymmetric mixing of singly excited states for increased entanglement fidelity at a smaller $G_{\text{hyb}}^{g} = G_{\text{hyb}}^{e}$ than for non-zero G_{hyb}^{e} and $G_{\text{hyb}}^{g} = 0$.

Appendix D. Level diagram evaluation

We seek to calculate the quality, specifically the efficiency η and fidelity $\mathcal{F}$, of the emitted photons *via* cascade decay from multiply excited states of cascade emitters. Assuming the desired photon state is $|\phi\rangle = \sum_{p}^{P} |p\rangle$ with density matrix $\sigma = |\phi\rangle\langle\phi|$, where, *e.g.*, $P = 2$ for the Bell and GHZ states we study in further detail in this manuscript, then both measures can be computed from the emitted photon density matrix ρ as [62]

$$\eta = (\sum_{p}^{P} \rho_{pp})/\text{Tr}[\rho], \tag{6}$$

$$\mathcal{F}(\rho', \sigma) = \left(\text{Tr}\sqrt{\sqrt{\rho'}\sigma\sqrt{\rho'}}\right)^2, \tag{7}$$

where $\rho' = \rho/\sum_p \rho_{pp}$. (Note that because the computed ρ is manually normalized in practice, we explicitly include $\text{Tr}[\rho]$ in Eq. (6).) Therefore, the efficiency η is the proportion of emitted photon states in one of the states $|p\rangle$ in the desired photon state $|\phi\rangle$, and the fidelity $\mathcal{F}$ is the overlap between the desired photon density matrix σ among the emitted photon states in the states $|p\rangle$.

We first show how to compute the full density matrix ρ of the emitted photons. Closely following a generalized version of the derivations shown in Refs. [63,64], a matrix element $\rho_{a,b}$ of the P-photon density matrix ρ can be written as

$$\begin{aligned} \rho_{a,b} &= \text{avg}[\langle \hat{\sigma}_{\omega_1^a}^{-}(t_1)\ldots\hat{\sigma}_{\omega_P^a}^{-}(t_P)\hat{\sigma}_{\omega_P^b}^{+}(t_P)\ldots\hat{\sigma}_{\omega_1^b}^{+}(t_1)\rangle] \\ &= \text{avg}(\mathcal{G}_{a,b}), \end{aligned} \tag{8}$$

where the average is over all times $t_1 < \ldots < t_P$; $q \in \{a, b\}$ refers to an P-photon state created by cascade emission of photons with frequencies $\omega_1^q, \ldots, \omega_P^q$; $\hat{\sigma}_{\omega}^{+}(t)$ $[\hat{\sigma}_{\omega}^{-}(t)]$ is the transition operator of the electronic transition $|l\rangle \rightarrow |m\rangle$ with frequency ω in the Heisenberg picture; and $\hat{\sigma}_{\omega}^{+} = \hat{a}_m^{\dagger}\hat{a}_l$ $[\hat{\sigma}_{\omega}^{-} = \hat{a}_l^{\dagger}\hat{a}_m]$.

Optics EXPRESS

$\mathcal{G}_{a,b}$ can be computed from the dynamics of the electronic system undergoing cascade decay. The diagonalized Hamiltonian of the electronic system, in the absence of interaction with the environment and determined *via* the procedure described in Section 2, is

$$\hat{H} = \sum_l E_l |l\rangle\langle l|, \tag{9}$$

where the lth eigenstate $|l\rangle$ has energy E_l. The evolution of the density operator ρ_{el} of the electronic system can be described with a master equation of the Lindblad form [65]:

$$\begin{aligned} \mathrm{i}\dot{\rho}_{\text{el}} &= \frac{1}{\hbar}[H, \rho_{\text{el}}] - \frac{\mathrm{i}}{2}\sum_\mu (\hat{L}_\mu^\dagger \hat{L}_\mu \rho_{\text{el}} + \rho_{\text{el}} \hat{L}_\mu^\dagger \hat{L}_\mu - 2\hat{L}_\mu \rho_{\text{el}} \hat{L}_\mu^\dagger) \\ &= \mathcal{L}[\rho_{\text{el}}], \end{aligned} \tag{10}$$

where the Lindblad operators $\hat{L}_\mu$ describe the interactions μ of the electronic system with the environment and $\mathcal{L}$ is the Liouville superoperator. As in Ref. [64], we consider two main forms of interaction with the environment in quantum dots, the physical emitters we suggest for further study: radiative decay, which leads to emission of frequency-entangled photons, and pure dephasing from electron-phonon coupling and spectral diffusion. We write the former Lindblad operators as $\hat{L}_{\text{r},lm} = \sqrt{\gamma_r^{lm}}|m\rangle\langle l|$. In agreement with Fermi's Golden Rule and Wigner-Weisskopf theory, we assume the radiative decay rate γ_r^{lm} for transitions from higher-energy state $|l\rangle$ to lower-energy state $|m\rangle$ is proportional to $|\boldsymbol{d}_{lm}|^2$ and scaled by a constant C. This constant C includes the photon density of states that, for simplicity, we assume to be constant for all photon frequencies, although this term could easily be generalized for any given cavity, waveguide, or free space configuration. For the dephasing process, we write the Lindblad operators as $\hat{L}_{\text{d},l} = \sqrt{\gamma_d}|l\rangle\langle l|$. For simplicity, we assume the dephasing rate γ_d is a constant, although this model could be straightforwardly generalized to describe the phenomenology of particular emitter systems. For instance, excitons in quantum dots or defects in solid-state materials both exhibit a zero-phonon line and a phonon tail that requires γ_d to be described more microscopically and potentially in a non-Markovian manner [66–68].

Using the quantum jump approach [69], we can solve the master equation to find

$$\rho_{\text{el}}(t) = e^{-\mathrm{i}\mathcal{L}t}\rho_{\text{el}}^0, \tag{11}$$

where ρ_{el}^0 is the initial density matrix at time $t = 0$ and asssumed to be decoupled from the environment. Finally, with $\rho_{\text{el}}(t)$, we can solve for $\mathcal{G}$ and, thus, the N-photon density matrix ρ using the quantum regression theorem [70,71] and noting that the operator $A_j(t_j)$ is evolved in the Heisenberg picture as $A_j(t_j) = e^{+\mathrm{i}\mathcal{L}t_j}A_j e^{-\mathrm{i}\mathcal{L}t_j}$:

$$\begin{aligned} \mathcal{G}_{a,b} = \mathrm{Tr}\Big[\hat{\sigma}^+_{\omega_P^b}(t_P)\Big[e^{-\mathrm{i}\mathcal{L}(t_P - t_{P-1})}\ldots\big[\hat{\sigma}^+_{\omega_1^b}(t_1) \\ \times[e^{-\mathrm{i}\mathcal{L}(t_1)}\rho_{\text{el}}^0]\hat{\sigma}^-_{\omega_1^a}(t_1)\big]\ldots\Big]\hat{\sigma}^-_{\omega_P^a}(t_P)\Big]. \end{aligned} \tag{12}$$

It is possible to further adapt this calculation to experimental conditions by including, for instance, the efficiency of detection. It is also possible to improve the entanglement by spectrally filtering the output or delaying the detection time, as described further in Ref. [64]. However, these approaches are outside the scope of this study, which aims to focus on the level structures of the composite emitters themselves. In addition, note that while the electronic density matrix only contains on-diagonal terms, the photonic density matrix can have off-diagonal terms that are affected by dephasing in the electronic system.

Optics EXPRESS

As computing the full photonic density matrix ρ can be resource-intensive, we seek a more efficient method of evaluating level diagrams. To this end, we observe that to compute η, we require only the on-diagonal elements of ρ, while $\mathcal{F}$ requires only the elements of ρ of the $|i\rangle$ bases. Consider the computational cost-savings when analyzing level diagrams for cascade emission of, for instance, GHZ states from $N = 3$ hybridized and dipole-coupled emitters. This system can have up to $\sim 10^5$ decay paths or unique photon states and, therefore, a density matrix with $\sim 10^5 \times 10^5$ matrix elements, while we require just $\sim 10^5$ matrix elements of ρ for η and only 4 elements are necessary for $\mathcal{F}$.

Computing all of the on-diagonal elements can still be an expensive process, however, as each requires a multidimensional integral over the product of several, potentially large matrices $\hat{\sigma}^{\pm}_{\omega}$ and linear maps $\exp(-i\mathcal{L}t)$. To more efficiently compute the on-diagonal elements of ρ, we turn to a classical rate equation approach. Given the diagonalized Hamiltonian and dipole operator in the eigenbasis, we determine all possible cascade decay pathways given some initial state, such as the N-excited state. With a general Runge-Kutta ordinary differential equation integrator, we propagate the rate equations $\mathrm{d}p_l/\mathrm{d}t = \sum_j (k^{\mathrm{in}}_{lm} p_m - k^{\mathrm{out}}_{lm} p_l)$, where rate constants k^{in}_{lm} (k^{out}_{lm}) $= C|\boldsymbol{d}_{lm}|^2$ for $E_l <$ (>) E_m, such that population transfer only from higher-energy to lower-energy states is allowed. As for the Lindbladian terms in the quantum master equation approach, both the scaling of k_{lm} with $|\boldsymbol{d}_{lm}|$ and the transfer of energy from higher-energy to lower-energy states is generally expected from spontaneous emission into free space calculated *via*, for instance, the Wigner-Weisskopf method or Fermi's Golden Rule, while C includes scaling due to the photon density of states that for simplicity we assume to be constant for all emitted photons.

A comparison of the time-dependent population curves computed with the classical vs. quantum approaches for two two-level emitters capable of emitting Bell states is shown as an example in Fig. 6 for initial population of $p_{ee}(t = 0) = 1$. For both approaches, the population briefly transfers to the intermediate states $|B_1\rangle$ and $|B_2\rangle$ before eventually populating the ground state $|g\rangle$. Note that the dark states are never populated. The results agree closely, suggesting that the classical rate equation approach is appropriate for computing populations and, therefore, on-diagonal terms of the photon density matrix ρ.

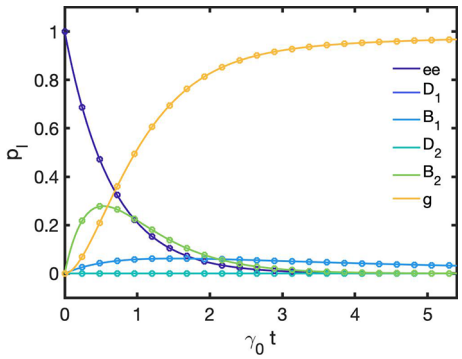

Fig. 6. Time-dependent population for cascade decay from the doubly excited state of two two-level systems using the quantum master equation (solid) and classical rate equation (circles) approaches. A schematic of such a level diagram is shown in the center of Fig. 1(b). The system is initialized with $p_{ee}(t = 0) = 1$. We set $\hbar\omega = 1$ eV, $d_x = |\boldsymbol{d}_1| = |\boldsymbol{d}_2| = 6$ e·Bohr, $\boldsymbol{r}_1 - \boldsymbol{r}_2 = 40\hat{i}$ in Bohr, $G^{\mathrm{e}}_{\mathrm{hyb}} = 80$ meV, and $\epsilon_r = 1$. The x-axis is unitless time, where the time t is scaled by the radiative rate $\gamma_0 = C|d_x|^2$ of the bare emitter. There is virtually zero difference in the time-dependent populations between the classical and quantum approaches in this case, enabling us to compute the on-diagonal terms of the photon density matrix ρ more efficiently with the classical approach.

Optics EXPRESS

From every state l, we then compute the relative outward flux $w_{lm} = \int k_{lm}^{\text{out}} p_l \mathrm{d}t / \sum_m \int k_{lm}^{\text{out}} p_l \mathrm{d}t$, where $\sum_m w_{lm} = 1$, of population from l into states m, allowing us to compute the relative population transfer through the path comprising of transitions through states $l \rightarrow \ldots \rightarrow n$ as $w_l \ldots w_n$. This product then corresponds to the on-diagonal photon density matrix element $\rho_{l,\ldots,n;l,\ldots,n}$, or the population in the photon state created by decay pathway $l \rightarrow \ldots \rightarrow n$.

Acknowledgements. The authors acknowledge valuable discussions with John Philbin, Stefan Ostermann, Valentin Walther, and Tomáš Neuman. D.S.W. is an NSF Graduate Research Fellow. S.F.Y. would like to acknowledge funding by DOE, AFOSR, and NSF.

Disclosures. The authors declare no conflicts of interest.

Data availability. Data underlying the results presented in this paper are not publicly available at this time but may be obtained from the authors upon reasonable request.

References

1. A. Einstein, B. Podolsky, and N. Rosen, "Can Quantum-Mechanical Description of Physical Reality Be Considered Complete?" Phys. Rev. **47**(10), 777–780 (1935).
2. J. S. Bell, "On the Einstein Podolsky Rosen Paradox," Physics **1**(3), 195–200 (1964).
3. S. J. Freedman and J. F. Clauster, "Experimental Test of Local Hidden-Variable Theories," Phys. Rev. Lett. **28**(14), 938–941 (1972).
4. L. K. Shalm, E. Meyer-Scott, B. G. Christensen, P. Bierhorst, M. A. Wayne, M. J. Stevens, T. Gerrits, S. Glancy, D. R. Hamel, M. S. Allman, K. J. Coakley, S. D. Dyer, C. Hodge, A. E. Lita, V. B. Verma, C. Lambrocco, E. Tortorici, A. L. Migdall, Y. Zhang, D. R. Kumor, W. H. Farr, F. Marsili, M. D. Shaw, J. A. Stern, C. Abellán, W. Amaya, V. Pruneri, T. Jennewein, M. W. Mitchell, P. G. Kwiat, J. C. Bienfang, R. P. Mirin, E. Knill, and S. W. Nam, "Strong Loophole-Free Test of Local Realism," Phys. Rev. Lett. **115**(25), 250402 (2015).
5. J. W. Pan, Z. B. Chen, C. Y. Lu, H. Weinfurter, A. Zeilinger, and M. Zukowski, "Multiphoton entanglement and interferometry," Rev. Mod. Phys. **84**(2), 777–838 (2012).
6. M. A. Nielsen and I. L. Chuang, *Quantum Computation and Quantum Information: 10th Anniversary Edition* (Cambridge University Press, USA, 2011), 10th ed.
7. S. Wehner, D. Elkouss, and R. Hanson, "Quantum internet: A vision for the road ahead," Science **362**(6412), 1 (2018).
8. M. Hillery, V. Bužek, and A. Berthiaume, "Quantum secret sharing," Phys. Rev. A **59**(3), 1829–1834 (1999).
9. M. A. Nielsen, "Cluster-state quantum computation," Rep. Math. Phys. **57**(1), 147–161 (2006).
10. P. G. Kwiat, S. Barraza-Lopez, A. Stefanov, and N. Gisin, "Experimental entanglement distillation and 'hidden' non-locality," Nature **409**(6823), 1014–1017 (2001).
11. D. C. Burnham and D. L. Weinberg, "Observation of simultaneity in parametric production of optical photon pairs," Phys. Rev. Lett. **25**(2), 84–87 (1970).
12. J. C. Howell, R. S. Bennink, S. J. Bentley, and R. W. Boyd, "Realization of the einstein-podolsky-rosen paradox using momentum and position-entangled photons from spontaneous parametric down conversion," Phys. Rev. Lett. **92**(21), 210403 (2004).
13. R. Horn, P. Abolghasem, B. J. Bijlani, D. Kang, A. S. Helmy, and G. Weihs, "Monolithic source of photon pairs," Phys. Rev. Lett. **108**(15), 153605 (2012).
14. A. Anwar, C. Perumangatt, F. Steinlechner, T. Jennewein, and A. Ling, "Entangled photon-pair sources based on three-wave mixing in bulk crystals," Rev. Sci. Instrum. **92**(4), 041101 (2021).
15. H. Takesue and K. Inoue, "Generation of polarization-entangled photon pairs and violation of bell's inequality using spontaneous four-wave mixing in a fiber loop," Phys. Rev. A **70**(3), 031802 (2004).
16. X. Lu, Q. Li, D. A. Westly, G. Moille, A. Singh, V. Anant, and K. Srinivasan, "Chip-integrated visible-telecom entangled photon pair source for quantum communication," Nat. Phys. **15**(4), 373–381 (2019).
17. E. Waks, E. Diamanti, B. C. Sanders, S. D. Bartlett, and Y. Yamamoto, "Direct Observation of Nonclassical Photon Statistics in Parametric Down-Conversion," Phys. Rev. Lett. **92**(11), 113602 (2004).
18. N. Akopian, N. H. Lindner, E. Poem, Y. Berlatzky, J. Avron, D. Gershoni, B. D. Gerardot, and P. M. Petroff, "Entangled photon pairs from semiconductor quantum dots," Phys. Rev. Lett. **96**(13), 130501 (2006).
19. A. Muller, W. Fang, J. Lawall, and G. S. Solomon, "Creating polarization-entangled photon pairs from a semiconductor quantum dot using the optical stark effect," Phys. Rev. Lett. **103**(21), 217402 (2009).
20. Y. Chen, J. Zhang, M. Zopf, K. Jung, Y. Zhang, R. Keil, F. Ding, and O. G. Schmidt, "Wavelength-tunable entangled photons from silicon-integrated iii-v quantum dots," Nat. Commun. **7**(1), 10387 (2016).
21. A. Orieux, M. A. Versteegh, K. D. Jöns, and S. Ducci, "Semiconductor devices for entangled photon pair generation: A review," Rep. Prog. Phys. **80**(7), 076001 (2017).
22. D. Huber, M. Reindl, J. Aberl, A. Rastelli, and R. Trotta, "Semiconductor quantum dots as an ideal source of polarization-entangled photon pairs on-demand: A review," J. Opt. **20**(7), 073002 (2018).
23. M. Zeeshan, N. Sherlekar, A. Ahmadi, R. L. Williams, and M. E. Reimer, "Proposed Scheme to Generate Bright Entangled Photon Pairs by Application of a Quadrupole Field to a Single Quantum Dot," Phys. Rev. Lett. **122**(22), 227401 (2019).

Optics EXPRESS

24. J. Liu, R. Su, Y. Wei, B. Yao, S. F. C. d. Silva, Y. Yu, J. Iles-Smith, K. Srinivasan, A. Rastelli, J. Li, and X. Wang, "A solid-state source of strongly entangled photon pairs with high brightness and indistinguishability," Nat. Nanotechnol. **14**(6), 586–593 (2019).
25. A. Fognini, A. Ahmadi, M. Zeeshan, J. T. Fokkens, S. J. Gibson, N. Sherlekar, S. J. Daley, D. Dalacu, P. J. Poole, K. D. Jöns, V. Zwiller, and M. E. Reimer, "Dephasing free photon entanglement with a quantum dot," ACS Photonics **6**(7), 1656–1663 (2019).
26. A. Ahmadi, A. Fognini, and M. E. Reimer, "Toward on-demand generation of entangled photon pairs with a quantum dot," in *Recent Advances in Nanophotonics-Fundamentals and Applications*, (IntechOpen, 2020).
27. M. Zukowski, A. Zeilinger, M. A. Horne, and H. Weinfurter, "Quest for GHZ states," Acta Phys. Pol. A **93**(1), 187–195 (1998).
28. M. Zwierz and P. Kok, "High-efficiency cluster-state generation with atomic ensembles via the dipole-blockade mechanism," Phys. Rev. A **79**(2), 022304 (2009).
29. M. Gimeno-Segovia, T. Rudolph, and S. E. Economou, "Deterministic Generation of Large-Scale Entangled Photonic Cluster State from Interacting Solid State Emitters," Phys. Rev. Lett. **123**(7), 070501 (2019).
30. N. H. Lindner and T. Rudolph, "Proposal for pulsed On-demand sources of photonic cluster state strings," Phys. Rev. Lett. **103**(11), 113602 (2009).
31. D. P. McCutcheon, N. H. Lindner, and T. Rudolph, "Error distributions on large entangled states with non-Markovian dynamics," Phys. Rev. Lett. **113**(26), 260503 (2014).
32. S. E. Economou, N. Lindner, and T. Rudolph, "Optically generated 2-dimensional photonic cluster state from coupled quantum dots," Ph.D. thesis (2010).
33. J. Roslund, R. M. De Araújo, S. Jiang, C. Fabre, and N. Treps, "Wavelength-multiplexed quantum networks with ultrafast frequency combs," Nat. Photonics **8**(2), 109–112 (2014).
34. H. Kim, H. J. Lee, S. M. Lee, and H. S. Moon, "Highly efficient source for frequency-entangled photon pairs generated in a 3rd-order periodically poled MgO-doped stoichiometric $LiTaO_3$ crystal," Opt. Lett. **40**(13), 3061 (2015).
35. N. Sangouard, C. Simon, H. de Riedmatten, and N. Gisin, "Quantum repeaters based on atomic ensembles and linear optics," Rev. Mod. Phys. **83**(1), 33–80 (2011).
36. D. S. Wang, M. Haas, and P. Narang, "Quantum interfaces to the nanoscale," ACS Nano **15**(5), 7879–7888 (2021).
37. C. Bernhard, B. Bessire, T. Feurer, and A. Stefanov, "Shaping frequency-entangled qudits," Phys. Rev. A **88**(3), 032322 (2013).
38. H. Yu, G. B. Liu, J. Tang, X. Xu, and W. Yao, "Moiré excitons: From programmable quantum emitter arrays to spin-orbit–coupled artificial lattices," Sci. Adv. **3**(11), 1–8 (2017).
39. N. J. Hestand and F. C. Spano, "Expanded Theory of H- and J-Molecular Aggregates: The Effects of Vibronic Coupling and Intermolecular Charge Transfer," Chem. Rev. **118**(15), 7069–7163 (2018).
40. J. Cui, Y. E. Panfil, S. Koley, D. Shamalia, N. Waiskopf, S. Remennik, I. Popov, M. Oded, and U. Banin, "Colloidal quantum dot molecules manifesting quantum coupling at room temperature," Nat. Commun. **10**(1), 5401 (2019).
41. D. S. Wang, T. Neuman, and P. Narang, "Dipole-Coupled Emitters as Deterministic Entangled Photon-Pair Sources," Phys. Rev. Res. **2**(4), 043328 (2020).
42. M. D. Lukin and P. R. Hemmer, "Quantum entanglement via optical control of atom-atom interactions," Phys. Rev. Lett. **84**(13), 2818–2821 (2000).
43. D. D. Dai, D. S. Wang, and P. Narang, "Passive controlled-variable phase gate on photonic qubits *via* cascade emitter," arXiv:2011.09302 (2020).
44. J. P. Philbin, J. Kelly, L. Peng, I. Coropceanu, A. Hazarika, D. V. Talapin, E. Rabani, X. Ma, and P. Narang, "Room temperature single-photon superfluorescence from a single epitaxial cuboid nano-heterostructure," arXiv:2104.06452 (2021).
45. Z. Ficek and R. Tanaś, "Entangled states and collective nonclassical effects in two-atom systems," Phys. Rep. **372**(5), 369–443 (2002).
46. D. L. Dexter, "A theory of sensitized luminescence in solids," J. Chem. Phys. **21**(5), 836–850 (1953).
47. P. L. Ardelt, K. Gawarecki, K. Müller, A. M. Waeber, A. Bechtold, K. Oberhofer, J. M. Daniels, F. Klotz, M. Bichler, T. Kuhn, H. J. Krenner, P. Machnikowski, and J. J. Finley, "Coulomb Mediated Hybridization of Excitons in Coupled Quantum Dots," Phys. Rev. Lett. **116**(7), 077401 (2016).
48. C. Hettich, C. Schmitt, J. Zitzmann, S. Kühn, I. Gerhardt, and V. Sandoghdar, "Nanometer resolution and coherent optical dipole coupling of two individual molecules," Science **298**(5592), 385–389 (2002).
49. Y. Zhang, Y. Luo, Y. Zhang, Y. J. Yu, Y. M. Kuang, L. Zhang, Q. S. Meng, Y. Luo, J. L. Yang, Z. C. Dong, and J. G. Hou, "Visualizing coherent intermolecular dipole-dipole coupling in real space," Nature **531**(7596), 623–627 (2016).
50. A. Naeem, F. Masia, S. Christodoulou, I. Moreels, P. Borri, and W. Langbein, "Giant exciton oscillator strength and radiatively limited dephasing in two-dimensional platelets," Phys. Rev. B **91**(12), 121302 (2015).
51. M. Khosla, S. Rao, and S. Gupta, "Polarons Explain Luminescence Behavior of Colloidal Quantum Dots at Low Temperature," Sci. Rep. **8**(1), 8385 (2018).
52. J. M. Elward and A. Chakraborty, "Effect of dot size on exciton binding energy and electron-hole recombination probability in CdSe quantum dots," J. Chem. Theory Comput. **9**(10), 4351–4359 (2013).
53. A. Carmele and S. Reitzenstein, "Non-Markovian features in semiconductor quantum optics: Quantifying the role of phonons in experiment and theory," Nanophotonics **8**(5), 655–683 (2019).

Optics EXPRESS

54. J. Förstner, C. Weber, J. Danckwerts, and A. Knorr, "Phonon-assisted damping of rabi oscillations in semiconductor quantum dots," Phys. Rev. Lett. **91**(12), 127401 (2003).
55. A. Nazir and D. P. McCutcheon, "Modelling exciton-phonon interactions in optically driven quantum dots," J. Phys.: Condens. Matter **28**(10), 103002 (2016).
56. E. V. Denning, J. Iles-Smith, N. Gregersen, and J. Mork, "Phonon effects in quantum dot single-photon sources," Opt. Mater. Express **10**(1), 222 (2020).
57. A. N. Poddubny, "Effect of continuous and pulsed pumping on entangled photon pair generation in semiconductor microcavities," Phys. Rev. B **85**(7), 075311 (2012).
58. D. Bauch, D. Heinze, J. Förstner, K. D. Jöns, and S. Schumacher, "Ultrafast electric control of cavity mediated single-photon and photon-pair generation with semiconductor quantum dots," Phys. Rev. B **104**(8), 085308 (2021).
59. S. P. Lukyanets and D. A. Bevzenko, "Effects of interatomic interaction on cooperative relaxation of two-level atoms," Phys. Rev. A **74**(5), 053803 (2006).
60. D. S. Wang, Í. Anali, and S. F. Yelin, "cascadeDecay," Github (2021), https://github.com/drekwang/cascadeDecay.
61. L. Ostermann, "Collective radiation of coupled atomic dipoles and the precise measurement of time," Ph.D. thesis, University of Innsbruck (2016).
62. R. Jozsa, "Fidelity for Mixed Quantum States," J. Mod. Opt. **41**(12), 2315–2323 (1994).
63. F. Troiani, J. I. Perea, and C. Tejedor, "Cavity-assisted generation of entangled photon pairs by a quantum-dot cascade decay," Phys. Rev. B **74**(23), 235310 (2006).
64. G. Pfanner, M. Seliger, and U. Hohenester, "Entangled photon sources based on semiconductor quantum dots: The role of pure dephasing," Phys. Rev. B **78**(19), 195410 (2008).
65. M. O. Scully and M. S. Zubairy, *Quantum Optics* (Cambridge University Press, 1997).
66. P. Borri, W. Langbein, S. Schneider, U. Woggon, R. L. Sellin, D. Ouyang, and D. Bimberg, "Ultralong dephasing time in InGaAs quantum dots," Phys. Rev. Lett. **87**(15), 157401 (2001).
67. B. Krummheuer, V. M. Axt, and T. Kuhn, "Theory of pure dephasing and the resulting absorption line shape in semiconductor quantum dots," Phys. Rev. B **65**(19), 195313 (2002).
68. K. D. Jahnke, A. Sipahigil, J. M. Binder, M. W. Doherty, M. Metsch, L. J. Rogers, N. B. Manson, M. D. Lukin, and F. Jelezko, "Electron-phonon processes of the silicon-vacancy centre in diamond," New J. Phys. **17**(4), 043011 (2015).
69. M. B. Plenio and P. L. Knight, "The quantum-jump approach to dissipative dynamics in quantum optics," Rev. Mod. Phys. **70**(1), 101–144 (1998).
70. C. W. Gardiner and P. Zoller, *Quantum noise: a handbook of Markovian and non-Markovian quantum stochastic methods with applications to quantum optics* (Springer, 2000).
71. G. Guarnieri, "Characterization of dynamical properties of non-Markovian open quantum systems," Ph.D. thesis, Universita Degli Studi di Milano (2017).